

Structural changes induced by metal electrode layers on ultrathin BaTiO₃ films

Y. Yacoby*

Racah Institute of Physics, Hebrew University, Jerusalem 91904, Israel

C. Brooks and D. Schlom

Department of Materials Science and Engineering, Pennsylvania State University, College Park, Pennsylvania 16802, USA

J. O. Cross and D. A. Walko

Advanced Photon Source, Argonne National Laboratory, Argonne, Illinois 60439, USA

C. N. Cionca, N. S. Husseini, A. Ripoșan, and R. Clarke

Department of Physics, University of Michigan, Ann Arbor, Michigan 48109-1120, USA

(Received 18 February 2008; revised manuscript received 20 April 2008; published 16 May 2008)

We have investigated the effect of evaporated gold electrodes on the structure of thin BaTiO₃ films grown epitaxially on a SrTiO₃ substrate. Two films, i.e., one five unit cell and the other ten unit cell thick, were studied. X-ray diffraction measurements analyzed by the coherent Bragg rod analysis (COBRA) method and diffuse x-ray scans show that the thinner film is pseudomorphic with respect to the substrate and very highly ordered, while the thicker one exhibits significant disorder and local discommensuration. The results further show that the ten unit cell film has an island morphology. The evaporation of 30 nm of gold had little effect on the thinner film, but it caused interesting and unexpected structural changes in the ten unit cell sample. In that case, the gold film drove the BaTiO₃ film closer to a pseudomorphic state and reduced the amount of disorder in the film. We attribute this behavior to surface tension forces applied by the gold to the BaTiO₃ structure. These results suggest a rather general conclusion, namely, that if the film and the evaporated electrode are smooth, the evaporated electrode has very little effect on the underlying structure. In contrast, if the film has an island-type morphology, the evaporated electrode exerts compressive stress on the islands.

DOI: [10.1103/PhysRevB.77.195426](https://doi.org/10.1103/PhysRevB.77.195426)

PACS number(s): 68.35.Gy

I. INTRODUCTION

Ferroelectric thin films are of increasing interest on account of the unusual dielectric phenomena associated with the interface to the substrate on which they are grown.¹ These effects include strain-modified polarization,² giant permittivities,³ and stripelike domain structures.⁴ In general, the strain resulting from lattice mismatch can couple to relevant excitations, such as soft modes and polar-spin excitations, to produce a rich variety of structures that do not have counterparts in the bulk phase. In some cases, ferroelectricity is enhanced,⁵ while in others, it is suppressed, depending on the details of the coupling to the order parameter.^{6,7}

Ferroelectric structures in thin film form have also been intensively investigated in the context of device applications,⁸ e.g., for electrical filters, nonvolatile information storage, and various types of thermal and mechanical sensors.¹ These technologies generally require some kind of electrode connection so that appropriate electrical boundary conditions can be established in order to switch, or modulate, the dielectric polarization by means of an external electric field.

There have been several studies^{9–11} to evaluate the effectiveness of different types of electrodes for ferroelectric thin film devices. One of the most interesting reported¹² that the fatigue of the switching polarization occurs with simple metallic electrodes, such as Pt, whereas metallic oxides, such as SrRuO₃, are effectively nonfatiguing electrodes. These and in the subsequent reports^{13,14} suggest that electrode materials may induce structural and chemical changes in ferroelectric

films, which will affect their performance in device applications. These effects have not yet been studied from a detailed structural point of view. In the present work, we bring to bear a powerful direct x-ray phasing technique, i.e., coherent Bragg rod analysis (COBRA),^{15,16} to probe the structure of ferroelectric thin films in the vicinity of the electrode and the interface with the substrate in an attempt to better understand the effects of placing an electrode on a perovskite ferroelectric material. Our findings are surprising and perhaps relevant to other electronic materials applications, such as patterned nanostructure surfaces and ultrathin semiconductor films and devices.

In this paper, the results reported show that the evaporation of a gold electrode on the surface of a BaTiO₃ film has a nontrivial effect on its structure. In particular, if the film grows in the form of islands, the evaporated gold can apply lateral compressive stress to each island by means of surface tension. This process can be quite general and may show up in a variety of thin film systems of relevance to device applications.

II. EXPERIMENTAL DETAILS**A. Sample preparation**

To study the effect of an evaporated electrode on the atomic structure of the BaTiO₃ films, we prepared two samples with different BaTiO₃ film thickness: one nominally five unit cell (UC) and the other ten UC thick. The films were grown on 1 × 1 cm² SrTiO₃ substrates by molecular-

beam epitaxy at a substrate temperature of 650 °C (measured by an optical pyrometer) in an oxygen background partial pressure of 5×10^{-7} Torr.¹⁷ Before growth, the (100) SrTiO₃ substrates were etched and annealed so that their uppermost surface was terminated by the TiO₂ monolayer.¹⁸ The BaTiO₃ films were deposited by using a shuttered growth process, in which the monolayer doses from Ba and Ti molecular beams were shuttered to grow alternating atomic layers of BaO and TiO₂.¹⁹ The fluxes of the Ba and Ti molecular beams were roughly determined by a quartz crystal microbalance and then fine tuned to yield the desired monolayer doses by monitoring the shuttered reflection high-energy electron diffraction intensity oscillations.²⁰ Film growth was initiated with the BaO monolayer of the first BaTiO₃ UC and terminated at the completion of the TiO₂ monolayer of the final UC to grow films with a total thickness of five and ten UCs.

The samples were then removed from the growth chamber and placed in an evaporation chamber, where first quarter of the area of the sample surface was evaporated with 30 nm of gold, the second quarter with 100 nm of aluminum, the third quarter with 10 nm of gold, while the fourth quarter was left bare. The results of the Al evaporated samples are similar to those of the 30 nm Au coated samples and will not be further discussed here.

B. X-ray measurement and analysis

We have investigated the structure of the BaTiO₃ films by using the COBRA phasing technique together with diffuse x-ray scattering (DXS). COBRA is a direct method for structural determination of epitaxial films and interfaces.^{15,16} It utilizes the continuous nature of the x-ray diffraction along Bragg rods normal to the film-substrate interface resulting from the lack of periodicity in this direction.

The experimental setup has been described in previous publications.^{16,21} In the present experiments, the point detector has been replaced by a line detector developed by Siddons.²² The line detector allowed us to measure the scattering along a line perpendicular to the Bragg rod. In this way, we could easily, and more efficiently, subtract the background to obtain the diffraction intensity along the Bragg rod. Moreover, the line detector also enabled us to measure the diffuse scattered radiation away from the Bragg rod. The DXS data provided us with very important additional information on the film structure.

The measurements were carried out at the Advanced Photon Source, Argonne National Laboratory, on beamline ID20. The samples were mounted on a Huber six-circle goniometer. Using an autocollimator mounted on the detector arm and a mirror mounted on the sample stage, we determined the orientations of the goniometer rotation axes. After feeding the orientation vectors to our LABVIEW control software system,²³ we tested the goniometer performance by measuring how well the autocollimator and mirror track each other under rotations around various axes. It was found that before calibration, the tracking could be as poor as 3 mrad, but the discrepancy decreased after calibration to about 0.3 mrad, which is sufficient for these experiments. The sample posi-

tion was then adjusted so that the goniometer center was on the sample surface.

The incident beam photon energy was set to 18 keV by using a standard liquid nitrogen-cooled Si double-crystal monochromator. The third harmonic from a type-A undulator was used with the beam width reduced to 200 μm and focused vertically using a Kirkpatrick-Baez (KB) mirror down to about 100 μm at the goniometer center. The beam orientation relative to the goniometer coordinate system was then accurately determined and fed to the LABVIEW control system. The sample orientation matrix relative to the goniometer coordinates was determined by using a number of Bragg reflections (usually 6). Using this orientation matrix, it was possible to go to any other Bragg point directly with an error less than a couple hundredths of a degree.

The diffraction along the [00L] Bragg rod was measured with equal incident and diffracted beam angles. In measuring the diffraction along all other Bragg rods, the incident beam angle was 5°. Before measuring the diffraction along a Bragg rod, the intensity profile was measured along a number of lines crossing the Bragg rod. The results were used to create a correction table that allowed us to measure the diffraction along the Bragg rods very accurately. The diffracted beam passed through an attenuation box²³ that was automatically controlled so that the attenuated beam was always within the dynamic range of the line detector. Special care was taken to ensure that the entire incident beam, which is monitored by a reference detector, impinged on the sample and the resulting diffracted beam was wholly measured by the detector. This ensured that the relative intensities within each Bragg rod and among the Bragg rods were correctly measured and normalized.

III. EXPERIMENTAL RESULTS

We measured the diffraction intensities along ten symmetry inequivalent Bragg rods. The results were then normalized by taking into account the incident and exit beam angles, as well as the beam polarization.²¹ One representative rod of the five UC sample and one of the ten UC sample are shown in Fig. 1. The positions along the rods are in reciprocal lattice units (rlu). Notice that the range of diffraction intensities, excluding the Bragg peaks, extends over 4 orders of magnitude. The results were analyzed by using the COBRA method. The starting reference structure consisted of an undeformed bulk SrTiO₃ structure and an undeformed tetragonal BaTiO₃ structure with the nominal number of UCs. After obtaining the electron density, we calculated the corresponding diffraction intensity and compared it to the measured diffraction intensities on all Bragg rods. As seen in Fig. 1, the calculated and measured intensities are in very good agreement with each other. Similar agreement was found in all other Bragg rods and samples.

The electron density of the five UC bare sample along lines perpendicular to the surface is shown in Fig. 2(a). The negative parts of the electron density are a result of inaccuracies in the experimental measurements and the COBRA analysis. Similar inaccuracies are expected in the positive values of the electron density. Note that the negative parts of

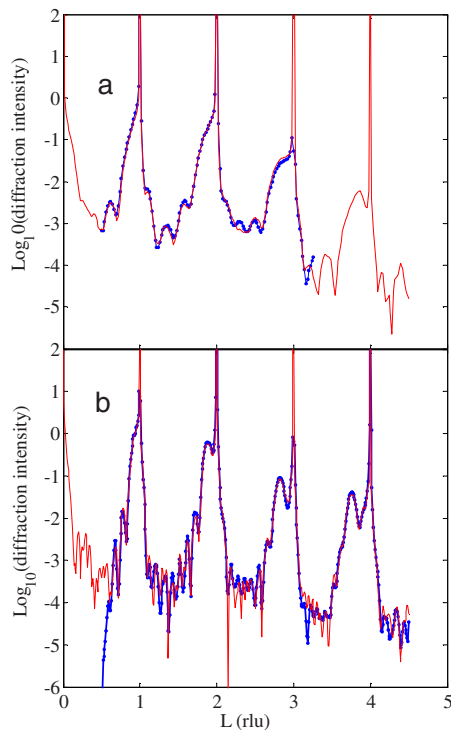


FIG. 1. (Color online) Diffraction intensity along the $[11L]$ Bragg rod of the bare samples. (a) five UC and (b) ten UC. Dots: experimental data; solid line: calculated profile from COBRA-determined electron density.

the electron density are very small. This and the fact that the calculated and measured diffraction intensities are in very good agreement means that the calculated electron density is very close to the real one. All the peaks occupy centrosymmetric positions, thus excluding the possibility that the film is in a single domain ferroelectric state. This result is quite different from the situation in PbTiO_3 ultrathin films. In particular, in a four UC thick PbTiO_3 film grown by metal-organic chemical vapor deposition, the film is in a single domain state and the atoms are at off-center positions.²¹ Theoretical work based on free energy calculations predicts both of these results.²⁴

The electron density profile of the bare five UC sample [Fig. 2(a)] shows a slight broadening and diminution of the three Ti peaks closest to the interface. This suggests some small distribution of the corresponding atomic positions. However, it is difficult to determine whether this is due to domain structure at the interface or arises from a small amount of positional disorder. Close to the surface, the Ba peak electron density decreases almost abruptly to zero. Notice that the Ba electron density drops before that of the Ti. This shows that the film is TiO_2 terminated. The electron densities of the 30 nm gold evaporated five UC thick film are shown in Fig. 2(b). The difference between this electron density and the electron density of the bare film is very small, which indicates that the effect of the Au evaporation is negligible.

Let us now consider the electron densities of the bare and gold evaporated ten UC BaTiO_3 film. These are shown in Figs. 3(a) and 3(b), respectively. The electron density map of

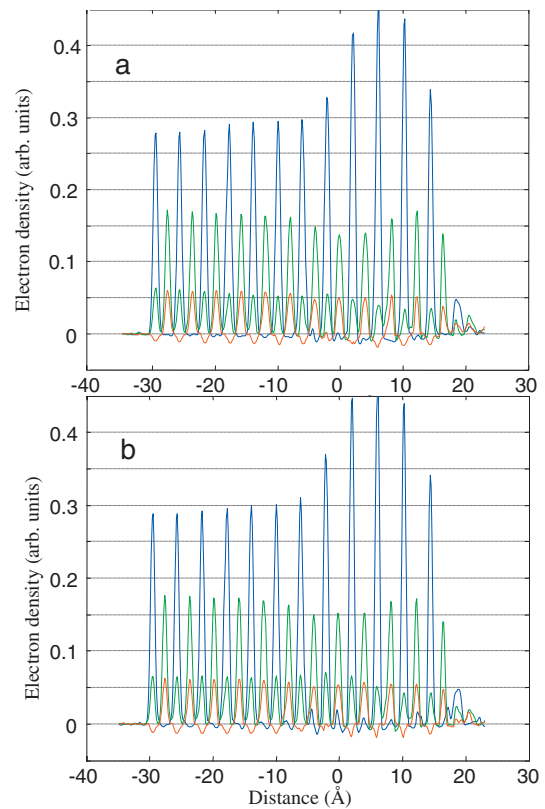


FIG. 2. (Color) Electron density of the bare five UC BaTiO_3 film along lines perpendicular to the film surface as a function of the distance from the nominal interface: (a) bare and (b) gold coated. The blue line going through Ba and Sr atoms, the green line going through Ti and O1 atoms, and the red line going through O2 atoms. The film surface and the bulk crystal are on the right and left hand sides, respectively. Eight nominal substrate unit cells are displayed with the top one at the interface, showing some Ba admixture.

this film is dramatically different from that of the five UC film. It takes more than two unit cells for the Ba electron density to decrease to zero at the film surface. This means that this film surface is rougher. However, here again, the Ba peaks decrease before the Ti ones, showing that the film is TiO_2 terminated. All the peaks of the Ba electron density in the film are smaller and broader than the corresponding ones in the five UC film. Significant changes can be seen even in the top two UCs of the substrate. The increased breadth and diminished peak heights indicate that the positions occupied by the atoms in the film significantly vary in different UCs. However, from COBRA alone, we cannot tell the correlation length of these distortions.

The electron density of the 30 nm gold evaporated sample shown in Fig. 3(b) is markedly different from that of the bare film. Systematically, all the peaks in the film are sharper and larger, suggesting that the Au BaTiO_3 film is more ordered and closer to a pseudomorphic structure than the bare film. From the COBRA-determined electron density profiles, we find that the average BaTiO_3 UC sizes in the perpendicular direction are larger than that of the substrate by factors of 1.061 and 1.070 for the five and ten UC samples, respec-

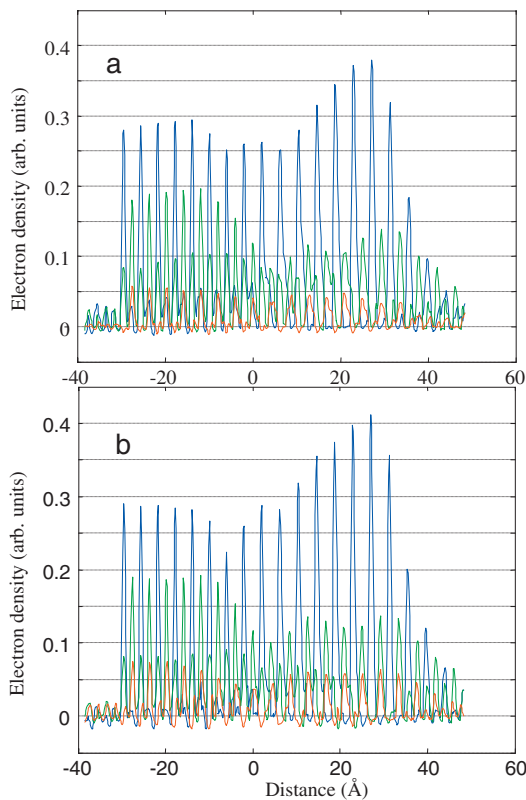


FIG. 3. (Color) Electron density of the bare ten UC BaTiO₃ film along lines perpendicular to the film surface as a function of the distance from the nominal interface: (a) bare and (b) gold coated. The blue line going through Ba and Sr atoms, the green line going through Ti and O1 atoms, and the red line going through O2 atoms. The film surface and the bulk crystal are on the right and left hand sides, respectively. Eight nominal substrate unit cells are displayed. The bottom six, on the bulk side, have essentially the bulk structure but the top two are smaller and broader, indicating the presence of significant disorder.

tively. This corresponds to Poisson ratios of 0.37 and 0.45, respectively.

The 10 nm thick gold film has an island morphology and its effect on the ten UC BaTiO₃ film is completely different from that of the thicker (30 nm) gold film. This can be seen in Fig. 4. This 10 nm gold film induces even more disorder. The negative values of the electron density are unusually large, indicating large uncertainties in the electron density. This could be a result of the presence of rather large gold islands on the order of the x-ray coherence length. In such a case, the COBRA analysis method is no longer strictly valid.²¹

Analysis of DXS data near the Bragg rods of the ten UC samples shows that the diffuse scattering has peaks along planes that contain the Bragg rod in question and the [00L] Bragg rod. Examples of the DXS intensity, which is along the line perpendicular to the [32L] Bragg rod and the diffracted beam, are shown in Fig. 5. The peaks of DXS of the ten UC samples are both displaced toward smaller k values with the displacement of the bare sample larger by about a factor of 1.55. The five UC samples practically show no diffuse scattering.

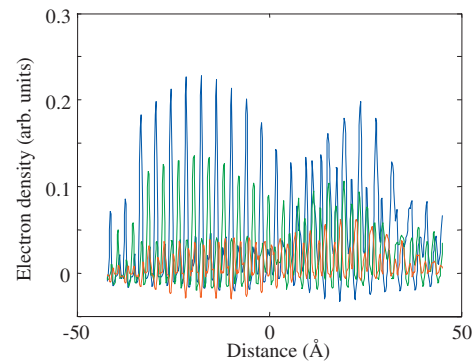


FIG. 4. (Color) Electron density of the 10 nm gold evaporated ten UC BaTiO₃ film along lines perpendicular to the film surface as a function of the distance from the nominal interface. The blue line going through Ba and Sr atoms, the green line going through Ti and O1 atoms, and the red line going through O2 atoms.

IV. DISCUSSION

The separation between the DXS peak and the axis center of the Bragg rod is proportional to the distance of the Bragg rod from the reciprocal space origin. This is shown in Fig. 6. Consequently, we interpret the DXS peaks to be a result of scattering by BaTiO₃ islands. Close to the interface, the islands are pseudomorphic with the substrate and they partially relax as the surface is approached. The average lateral UC size is somewhat larger than that of the substrate. The difference can be determined from the slope in Fig. 6. The average BaTiO₃ in-plane lattice spacing is about 0.016 Å larger than that of the substrate. We have previously shown that layers that are not in the registry with the substrate do not show up in the COBRA-determined electron density.¹⁶ The fact that the electron density peaks are observed even at the surface means that even the relaxed part is still in registry with the substrate although the atoms are somewhat displaced relative to the corresponding atoms in the substrate. This means that the relaxation is elastic. The DXS peak width is inversely

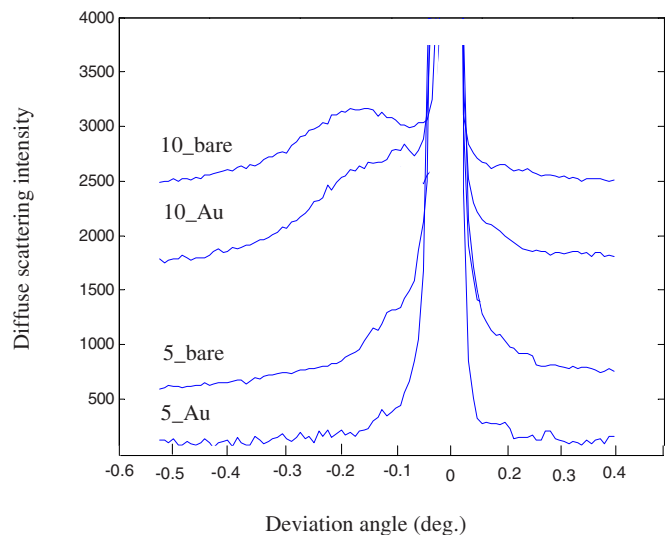


FIG. 5. (Color online) Diffuse x-ray scattering along the line perpendicular to the [32L] Bragg rod and the diffracted beam.

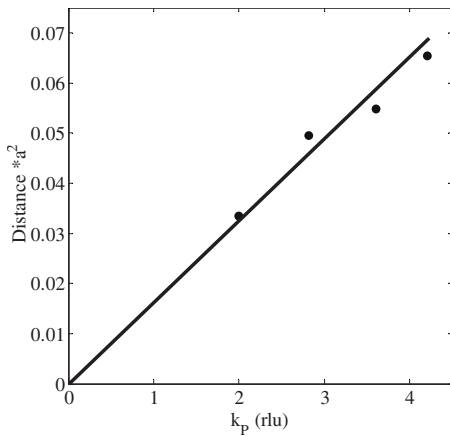


FIG. 6. The separation between the DXS peak and the Bragg rod (measured in \AA^{-1}) multiplied by the square of the in-plane UC (measured in \AA^2) as a function of the distance of the Bragg rod from the origin expressed in rlu. The slope is equal to the average difference between the BaTiO_3 UC and the substrate one.

proportional to the size of the BaTiO_3 islands. The bare ten UC film islands are about $N_{is}=36$ UC long. Direct evidence for island growth of BaTiO_3 on SrTiO_3 has been observed by using cross-section transmission electron microscopy.²⁵ Since the structure in the islands is partially relaxed, translating all the atoms into one substrate-defined UC by using substrate-defined UC vectors results in a folded structure²⁶ with the atomic electron density peaks having a full width at half maximum of about $0.016 \times 36 = 0.57 \text{ \AA}$.

The COBRA-determined half width of the folded Ba atom electron density is shown in Fig. 7 for both gold covered and bare samples with five and ten UC thicknesses. One sees that the width of the folded structure of the five UC samples is practically unchanged, while that of the bare ten UC sample changes by about 0.06 \AA . The Sr electron density in the

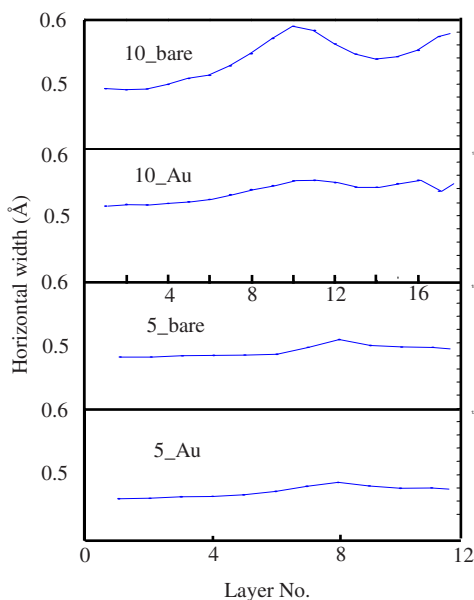


FIG. 7. (Color online) The horizontal half width of the Ba atom electron density peak as a function of the UC number.

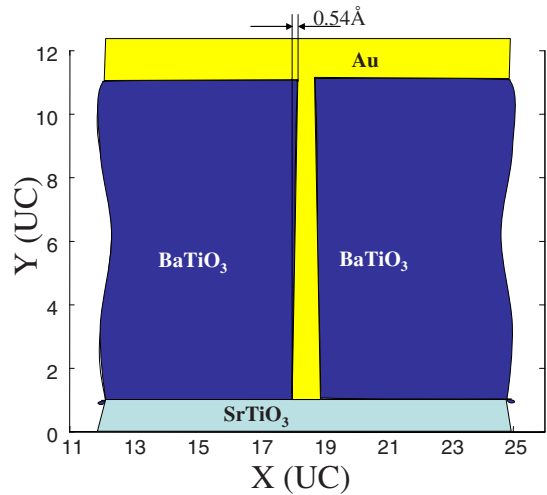


FIG. 8. (Color online) The shape of the islands as calculated from elasticity theory. The relaxation at the top corner is about 0.54 \AA . Therefore, on the average, the islands are approximately 0.54 \AA wider than at the base.

substrate provides the instrumental peak width. Thus, the COBRA-determined width of the Ba folded structure $W_C = 2(0.562^2 - 0.5^2)^{1/2} = 0.5 \text{ \AA}$, which is in good agreement with the value found from the diffuse scattering measurement. The corresponding value for the gold covered sample is $W_C = 2(0.54^2 - 0.51^2)^{1/2} = 0.35 \text{ \AA}$. Namely, the islands under the gold have been squeezed by about 0.15 \AA . This is also in agreement with what we observe from DXS.

An idealized picture of the island morphology observed in Ref. 25 is shown in Fig. 8. Very close to the substrate, the in-plane UC size of BaTiO_3 is expected to be equal to that of the substrate and to expand as one goes further away from the substrate. We used bulk compression ($\sigma_{1111} = 10.8 \times 10^{-12} \text{ m}^2/\text{N}$) and shear ($\sigma_{1212} = 7.98 \times 10^{-12} \text{ m}^2/\text{N}$) compliances²⁷ to calculate this expansion. The results are shown in Fig. 8. From this calculation, the average change in the UC dimension is $\Delta_e = 0.015 \text{ \AA}$, which is in good agreement with the value determined from DXS.

Let us consider now the effect of the evaporated gold on the five and ten UC films. The fact that the thick gold has practically no effect on the structure of the five UC film suggests that if both BaTiO_3 and gold films were smooth (no islands), then the strain induced by the gold would be small. On the other hand, if the gold film has an island morphology, it would apply nonuniform strain on the BaTiO_3 film, causing significant disorder in the atomic positions in the film.

The case of the 30 nm gold film evaporated on the ten UC thick BaTiO_3 film is particularly interesting. As explained above, the BaTiO_3 film has an island morphology. Thus, when gold is evaporated, it wets the islands mesas and penetrates in between the islands. Slightly compressing the islands mesas in the lateral directions decreases the gold island interface area, lowering the interface energy. This exerts pressure on the islands in the lateral directions, leading to a decrease in the BaTiO_3 UC size and driving it closer to the pseudomorphic state. Consequently, the nonuniform strains are decreased, leading to larger and narrower electron density peaks, as observed.

To check the validity of this argument, we have compared an order of magnitude estimate of the surface energy gained by squeezing the islands to the elastic energy required for the same squeeze. The surface energy is

$$E_S = SL\Delta. \quad (1)$$

The elastic energy is approximately equal to

$$E_E = H\Delta^2/2\sigma_{1111}, \quad (2)$$

where H is the film thickness and Δ is the extent to which the island has been squeezed. Using the bulk value for surface tension $S=1$ N/m and $L/H=4$, we find that for the measured value of $\Delta \approx 0.15$ Å, $E_S/E_E=5.6$. This means that the gain in surface tension energy is more than that required in order to account for the compression of the islands by the gold.

V. SUMMARY AND CONCLUSIONS

Up to about five UCs, BaTiO₃ grows as a purely pseudomorphic epitaxial film. The film is fully strained so its lateral UC dimension is equal to that of the substrate. To within the experimental error, the electron density of the folded structure is as expected for an ideal epitaxial film. Evaporating a relatively thick gold film essentially does not change the film structure.

Between five and ten UCs, the BaTiO₃ film develops an island morphology. The in-plane lattice spacings within the islands are partially relaxed. From DXS, the average lateral UC size is larger than that of the substrate by about 0.016 Å and the average size of the islands is about 36 substrate UCs, namely, about 140 Å. The COBRA measured folded electron density peak in this case, at 0.5 Å, is broader than that of the substrate and compares well to the value calculated

from the DXS measurements, 0.57 Å. In this case, the gold evaporated film has a large effect on the film atomic structure. The gold coats the surface of the island mesas and penetrates into the crevices between the islands, applying lateral stress to the islands and causing the BaTiO₃ UC to decrease. In this way, the film becomes closer to being pseudomorphic with the substrate. This change in structure is clearly seen in the COBRA-determined electron density maps as well as the diffuse scattering profiles.

In this paper, the results presented suggest some more general conclusions. (1) The evaporation of gold or other electrodes on a smooth epitaxial film is expected to have very little effect on the atomic structure of the epitaxial film in spite of the fact that the electrode itself may be strained. (2) If the epitaxial film has island morphology, or has a dense set of crevices, or has short length-scale roughness, the evaporated electrode can affect the atomic structure of the film. In some particular cases, such as island morphology or nanoscale patterning, the effect of the electrode may be to apply lateral compressive strain on each island. This strain tends to decrease the area of the island and to increase the spacing between islands. (3) If the electrode is very thin such that it is no longer uniform, the electrode will have a large effect introducing a significant structural disorder in the vicinity of the electrode.

ACKNOWLEDGMENTS

This work was supported in part by the U.S. Department of Energy under Grant No. DE-FG02-06ER46273. Use of the Advanced Photon Source was supported by the Office of Science, Office of Basic Energy Sciences, U.S. Department of Energy under Contract No. DE-AC02-06CH11357.

*yizhak@vms.huji.ac.il

¹M. Dawber, K. M. Rabe, and J. F. Scott, *Rev. Mod. Phys.* **77**, 1083 (2005).
²W. Tian, J. C. Jiang, X. Q. Pan, J. H. Haeni, Y. L. Li, L. Q. Chen, D. G. Schlom, J. B. Neaton, K. M. Rabe, and Q. X. Jia, *Appl. Phys. Lett.* **89**, 092905 (2006).
³A. Erbil, Y. Kim, and R. A. Gerhardt, *Phys. Rev. Lett.* **77**, 1628 (1996).
⁴S. K. Streiffer, J. A. Eastman, D. D. Fong, C. Thompson, A. Munkholm, M. V. Ramana Murty, O. Auciello, G. R. Bai, and G. B. Stephenson, *Phys. Rev. Lett.* **89**, 067601 (2002).
⁵K. J. Choi, M. Biegalski, Y. L. Li, A. Sharan, J. Schubert, R. Uecker, P. Reiche, Y. B. Chen, X. Q. Pan, V. Gopalan, L. Q. Chen, D. G. Schlom, and C. B. Eom, *Science* **306**, 1005 (2004).
⁶N. A. Pertsev, A. G. Zembilgotov, S. Hoffmann, R. Waser, and A. K. Tagantsev, *J. Appl. Phys.* **85**, 1698 (1999).
⁷Y. Yacoby, Y. Girshberg, E. A. Stern, and R. Clarke, *Phys. Rev. B* **74**, 104113 (2006).
⁸C. H. Ahn, K. M. Rabe, and J. M. Triscone, *Science* **303**, 488 (2004).
⁹C. Dearaujo, J. D. Cuchiaro, L. D. McMillan, M. C. Scott, and J.

F. Scott, *Nature (London)* **374**, 627 (1995).

¹⁰R. E. Jones, *Solid State Technol.* **40**, 201 (1997).
¹¹T. Tsurumi, T. Ichikawa, T. Harigai, H. Kakemoto, and S. Wada, *J. Appl. Phys.* **91**, 2284 (2002).
¹²C. B. Eom, R. B. Vandover, J. M. Phillips, D. J. Werder, J. H. Marshall, C. H. Chen, R. J. Cava, R. M. Fleming, and D. K. Fork, *Appl. Phys. Lett.* **63**, 2570 (1993).
¹³D. H. Do, P. G. Evans, E. D. Isaacs, D. M. Kim, C. B. Eom, and E. M. Dufresne, *Nat. Mater.* **3**, 365 (2004).
¹⁴X. J. Lou, M. Zhang, S. A. T. Redfern, and J. F. Scott, *Phys. Rev. Lett.* **97**, 177601 (2006).
¹⁵Y. Yacoby, M. Sowwan, E. A. Stern, J. O. Cross, D. Brewes, R. Pindak, J. Pitney, E. B. Dufresne, and R. Clarke, *Nat. Mater.* **1**, 99 (2002).
¹⁶M. Sowwan, Y. Yacoby, J. Pitney, R. MacHarrie, M. Hong, J. Cross, D. A. Walko, R. Clarke, R. Pindak, and E. A. Stern, *Phys. Rev. B* **66**, 205311 (2002).
¹⁷C. D. Theis and D. G. Schlom, *J. Cryst. Growth* **174**, 473 (1997).
¹⁸G. Koster, B. L. Kropman, G. J. H. M. Rijnders, D. H. A. Blank, and H. Rogalla, *Appl. Phys. Lett.* **73**, 2920 (1998).

- ¹⁹D. G. Schlom, J. H. Haeni, J. Lettieri, C. D. Theis, W. Tian, J. C. Jiang, and X. Q. Pan, *Mater. Sci. Eng., B* **87**, 282 (2001).
- ²⁰J. H. Haeni, C. D. Theis, and D. G. Schlom, *J. Electroceram.* **4**, 385 (2000).
- ²¹D. D. Fong, C. Cionca, Y. Yacoby, G. B. Stephenson, J. A. Eastman, P. H. Fuoss, S. K. Streiffer, C. Thompson, R. Clarke, R. Pindak, and E. A. Stern, *Phys. Rev. B* **71**, 144112 (2005).
- ²²P. Siddons (private communication).
- ²³Y. Yacoby, D. Brewes, M. Bretschneider, M. Sowwan, R. Clarke, R. Pindak, and E. A. Stern, in *Synchrotron Radiation Instrumentation: Eighth International Conference*, edited by T. Warwick, J. Arthur, H. A. Padmore, and J. Stohr, AIP Conf. Proc. No. 705 (AIP, New York, 2004), p. 1221.
- ²⁴Y. Yacoby, Y. Girshberg, E. A. Stern, and R. Clarke, *Phys. Rev. B* **74**, 104113 (2006).
- ²⁵A. Visinoiu, M. Alexe, H. N. Lee, D. N. Zakharov, A. Pignolet, D. Hesse, and U. Gosele, *J. Appl. Phys.* **91**, 10157 (2002).
- ²⁶Y. Yacoby, R. Pindak, R. MacHarrie, L. Peiffer, L. Berman, and R. Clarke, *J. Phys.: Condens. Matter* **12**, 3929 (2000).
- ²⁷E. Poindexter and A. A. Giardini, *Phys. Rev.* **110**, 1069 (1958).